A. G. Evans, A. H. Heuer and D. L. Porter

Fracture 1977, Volume 1, ICF4, Waterloo, Canada, June 19 - 24, 1977

THE FRACTURE TOUGHNESS OF CERAMICS

A. G. Evans*, A. H. Heuer** and D. L. Porter**

ABSTRACT

Recently proposed approaches for enhancing the toughness of ceramics have been examined. Several approaches have been demonstrated to produce appreciable increases in toughness, including (a) controlled microfracture, (b) coherent precipitation, (c) ductile second phase networks, and (d) stress induced phase transformations. The relative merits and limitations of each approach, and the important prerequisites for optimum toughening, have been discussed.

1. INTRODUCTION

It has long been recognized that many of the unique properties of ceramics, e.g., their hardness and refractoriness, could be used to advantage if the limitations on structural integrity, imposed by an innate brittleness, could be circumvented. Several approaches to this problem are possible, as summarized in a recent review [1]. The approach that is being most extensively utilized (for the application of ceramics in turbines, as bearings, insulators, etc.) is (i) to develop materials with an acceptable long-term strength by minimizing the susceptibility to slow crack growth, (ii) to eliminate the most deleterious fabrication defects (inclusions, pores, etc.), by improved fabrication technology, and (iii) to apply failure prediction techniques such as overload proof testing [1,2]. However, very little attention has been devoted to enhancing the strength and crack arrest capabilities by optimizing the fracture toughness. Yet, recent developments [3,4,5,6] have indicated that significant increases in the toughness of ceramics should be possible, and this topic promises to be a fruitful research and development area for several years. It is the intent of this paper, therefore, to carefully examine each of the toughening mechanisms that might pertain to ceramics (Table I), as needed to establish guidelines for microstructural design studies.

The paper will thus be organized in the following sequence. We first review the criteria for crack extension in very brittle materials and then outline and examine the possible approaches for enhancing toughness in terms of the crack extension criteria. Finally, suggestions concerning the most promising approaches for toughness enhancement will be made.

2. CRACK EXTENSION CRITERIA

In ceramic polycrystals, crack tip deformation (when it occurs) does not normally produce the general homogeneous strain needed to achieve crack blunting, [1,7] and macrocrack propagation is usually considered to involve

*Science Center, Rockwell International, Thousand Oaks, CA 91360, U.S.A.
**Case Western Reserve University, Cleveland, OH 44106, U.S.A.

a direct bond rupture process at the crack tip, as depicted in Figure 1* Evaluation of the crack extension process thus entails a determination of the stress conditions that prevail when the displacement, u, of the bonds at the crack tip reaches the critical bond rupture displacement, u_c.

For crack extension by bond rupture at a critical displacement, u_c, Lawn and Wilshaw [8] have used Barenblatt's notion [9] of a non-linear elastic zone ahead of the crack tip to derive the following equality;

$$G_c = 2\int_0^{u_c} \sigma(u)\, du \qquad (1)$$

where $\sigma(u)$ is the stress that derives from the force-displacement function for bond rupture (Figure 1) and G_c is a critical value of the strain energy release rate. The strain energy release rate is thus expected to be the key parameter defining crack extension in most ceramic polycrystals. Hence, by noting the relations between G and the stress intensity factor K [8],

$$K^2 = EG \quad \text{(plane stress)} \qquad K^2 = \frac{EG}{1-\nu^2} \quad \text{(plane strain)} \qquad (2)$$

(where E is Young's modulus and ν is Poisson's ratio) and the relation between K and the principal tensile stresses (σ_1, σ_2) [10]

$$\sigma_{1,2} = \frac{K}{\sqrt{2\pi r}} \cos\theta/2(1\pm\sin\theta/2) \qquad (3)$$

(where r is the distance from the crack tip and θ is the angle relative to the crack plane), it is apparent that stress field determinations provide a direct method for analyzing crack extension behavior. Consequently, crack extension will be evaluated herein by deriving G, the strain energy release rate, from stress field analyses; but for those cases where elastic modulus effects are thought to play a relatively unimportant role in the toughening process, crack extension will be evaluated directly in terms of K, the stress intensity factor.

The interactions between the stress field of a primary crack and the stress developed by microstructural changes that occur in a zone around the crack tip are complex. Numerical solutions are available for a few two dimensional problems, but rigorous analyses of the total stress field are rarely possible. It is generally required, therefore, that solutions for simplified analogies be sought so as to establish guidelines which can be verified and quantified using empirical techniques. Additionally, it is sometimes informative to appeal to the thermodynamics of the crack extension process. However, this approach can be misleading unless the First Law energy balance is considered in toto. It is usually adequate to consider the 'fixed grip' situation, which can be written in the form [1,8]

*In the exceptional cases where crack blunting can occur, this relatively simple picture of the crack extension process may not apply; rather, the propagation of secondary cracks formed in a zone ahead of the primary crack may be the critical stage in the crack extension sequence.

$$\frac{\partial}{\partial A_c}(U_\sigma + U_s + U_p) = 0 \qquad (4)$$

where A_c is the crack area, U_σ is the strain energy, U_s is the energy of the newly formed surfaces (this includes the thermal and strain energy changes associated with crack tip plasticity, if it occurs) and U_p is a term, referred to herein as the phonon energy, which includes the energy associated with the stress waves (manifested as acoustic emission) emitted by the propagating crack. The major limitation of the thermodynamic approach is its inability to effectively determine changes in U_p. Nevertheless, it is usually rewarding to examine the changes expected in U_σ and U_s to derive possible trends in the resistance to crack propagation.

In all crack propagation processes, the change in strain energy due to the increase in the macrocrack length (which is negative for the fixed grip condition) and the increase in the energy associated with the macrocrack surface, must be included. For a through crack of unit thickness [1,8];

$$\frac{\partial U_\sigma}{\partial A_c} = \frac{-2\pi\sigma_A^2 a}{E} \qquad \frac{\partial U_s}{\partial A_c} = 4\Gamma \qquad (5)$$

where σ_A is the applied stress, a is the crack length and Γ is the average 'surface energy' per unit projected area of macrocrack surface (which again includes plastic work if this is involved in the fracture process). Additional processes that occur near the crack tip, which change the strain or surface energies of the system, can thereafter be incorporated in the energy balance (equation 4) to determine whether the stress for crack propagation, σ_A, is likely to be altered (as discussed in more detail later), *assuming* that changes in U_p are relatively small.

3. DISLOCATION EFFECTS

The interaction of dislocations with cracks has been observed in single cyrstals of ionically-bonded solids [11,12,13,14,15], and the nature of the dislocation/crack interaction has been explored in detail. The most important result for present purposes is that the toughness increases as the dislocation flow stress (τ_c) increases [14,15], because crack extension is "triggered" by dislocation phenomena that produce a stress enhancement at the crack tip.

Dislocation motion may also play an analogous role in the fracture of polycrystals, although the detailed dislocation/crack interaction mechanism may be quite different. To comprehend the role of the dislocation activity (if it occurs), it is useful to construct the plane stress principal tensile stress field around a crack (from equation 3), as shown in Figure 2. From such a stress field it is possible to envisage dislocation activity initiating at grain boundary sources and progressing to adjacent boundaries, where a pile-up and resultant microfracture may occur. Two such possibilities are depicted in Figure 3. Pile-ups of type (1), where the slip plane "cuts across" the crack plane, may be possible, even though the shear

stress is zero at the crack plane,* if the leading dislocations can be forced across this plane by the succeeding dislocations emitted at S_1. Type (2) pile-ups, where the slip planes are parallel to the crack plane, are more favourable because relatively large shear stresses can exist over the entire dislocation path. Microcrack initiation at the grain boundary due to dislocation pile-ups can occur, in the manner described by Stroh [16], provided that the stress due to pile-up orthogonal to the prospective microfracture plane (generally the grain boundary) is tensile. Since the tangential stress ahead of the pile-up has an angular dependence $f(\phi)$ given by [16] (see Figure 3);

$$f(\phi) = \sin\phi \cos\phi/2 \tag{6}$$

the stress will be tensile for $o < \phi < \pi$ with a maximum at $\phi = 0.39\ \pi$. Microcracks can thus develop at both Type (1) and (2) pile-ups, in the directions indicated in Figure 3, if the pile-up stresses reach the necessary intensity. Further, since the stresses around the primary crack in a direction orthogonal to the microcrack plane are tensile (Figure 2), linkage of the microcracks with the primary crack, which constitutes an extension of the primary crack, would be possible. An analysis of this process has been performed [1] for the condition where the first slip band formed in the crack tip zone creates a microcrack, which then links directly with the primary crack to cause crack extension. For this condition, the dislocations do not significnatly perturb the stress field around the primary crack and the conventional crack tip elastic stress field equations (e.g. equation 3) can be used. The analysis indicates that K_c is related to the critical resolved shear stress for dislocation flow, τ_c, by [1];

$$K_c = k_1\ \tau_c + k_2 \sqrt{bEK_B} \tag{7}$$

where b is the Burgers vector, K_B is the grain boundary fracture toughness, and k_1 and k_2 are parameters that depend on the grain diameter, D_g. For a Type (1) source, D_g enters k_1 as a numerator term [1]; while for a Type (2) source, D_g may also enter k_2 as a denominator term. Thus, the grain size dependence of K_c is uncertain. However, a direct dependence of K_c on τ_c is an essential feature of this process, and hence, the toughness should increase as the dislocation flow stress increases, as observed in single crystals.

If more extensive dislocation activity precedes microcrack initiation, the dislocations can reduce the stress at the primary crack and K_c could be larger than indicated by equation (7). An analysis of this problem is complex and is sensitive to such details as the dislocation source density, distribution and activation stress, the propensity for cross slip, etc. Since these are generally not known for ceramic polycrystals, it is relatively unrewarding to pursue the details of the analysis; it is adequate to recognize that K_c can, in certain real cases, exceed the value suggested by equation (7).

It has been suggested by some researchers that dislocation activity does play a role in crack extension in ceramic polycrystals (normally considered

*This is less of a restriction very close to the crack tip where the biaxiality is reduced by the presence of the free surface.

brittle), but many others argue that dislocation motion may only be important at relatively high temperatures ($\gtrsim 800^0$C). It is very difficult to provide a fully convincing argument for, or against, the role of dislocation activity. However, perhaps the most persuasive indications presently available are the direct observations of crack tip dislocation activity in alumina by Wiederhorn et al [17], using transmission electron microscopy. These indicate that *observable* dislocation activity does not occur below $\sim 800^0$C. Additionally, the temperature independence of K_c observed for most ceramic polycrystals below this temperature [18,19,20] would be difficult to explain in terms of dislocation-assisted crack propagation, because τ_c is strongly temperature dependent in this range [1]. Hence, we tend in this paper to discount the possible role of dislocation activity in the crack extension process in most ceramic polycrystals, and devote more attention to toughening mechanisms that do not invoke crack tip plasticity. However, we do not intend to convey the impression that toughening by homogeneous crack tip plasticity may not be possible in some ceramic polycrystals (especially at elevated temperatures).

4. MICROCRACKING

Microcracking is frequently observed to occur in two phase ceramics [21] or in single phase ceramics with anisotripic thermal expansion or elastic properties [20]. It has thus been postulated [5,22,23] that microcracking can occur in the vicinity of a macrocrack tip to generate a 'process zone'. Should this occur, the fracture toughness of the ceramic would certainly differ from that expected in the absence of such microfracture. To comprehend the consequences of microcracking, it is necessary to examine probable microfracture distributions, and then to determine the effect of these on the stress distribution around the primary crack and on the energetics of fracture.

4.1 Microcrack distribution

Microfracture in a given material is expected to occur over a range of stress. It is thus convenient for the analysis of microfracture to define a microfracture distribution function, which determines the probability, Φ, that a microcrack precursor will be activated. An extreme value function [24] is a pertinent choice, and herein we use

$$\Phi = 1 - \exp(-S/S_o)^m \tag{8}$$

where S is the applied stress at microfracture under uniaxial tension, and S_o and m are location and scale parameters, respectively. Equation (8) reduces at small Φ to a form;

$$\Phi = \left(\frac{S}{S_o}\right)^m \tag{9}$$

which has been shown to apply to the microfracture detected by acoustic emission during flexural testing [20,21,25]. The spatial distribution of microcracks around a primary crack can be determined from equation (8) and the principal tensile stress field (equation 3), if it is assumed that microcrack interaction does not occur (this point is discussed later). However, in order to avhieve this, the microfracture probability under biaxial tension must firstly be derived from the uniaxial microfracture distribution (equation 8). This could either be achieved empirically, or

by using a modification* of the approach used by Batdorf and Crose [26] to determine macrofracture probabilities in polyaxial stress states. Then, the modified spatial character of the stress field around the primary crack that accompanies the development of the microcrack zone must be deduced. Both steps entail complex computations, which are not attempted herein, because a useful physical picture of the role of microfracture in macrocrack extension can be provided by simply assuming that the stress field is uniaxial, with the stress given by;**

$$\sigma = \beta \frac{K_I}{\sqrt{2\pi r}} \qquad 0 < \theta < 0.7\pi$$
$$\sigma = 0 \qquad 0.7\pi < \theta < \pi \tag{10}$$

where β is a constant (≈ 1) determined by the average value of the angular dependence of the principal tensile stress (see Figure 2). Equating σ to S (the microfracture condition assumed herein) and noting that

$$\Phi \approx \rho/\rho_o \tag{11}$$

where ρ is the microcrack density and ρ_o is the density of microcrack sources, we obtain from equations (8) and (10)

$$\frac{\rho}{\rho_o} \approx 1 - \exp\left[-\left(\frac{\beta K_I}{\sqrt{2\pi}\ S_o}\right)^m r^{-m/2}\right] \qquad 0 < \theta < 0.7\pi \tag{12}$$

It is immediately apparent from this relation that since m is usually a positive integer (e.g. for mortar [25], porcelain [21], and alumina [20], m = 2, 4, and 12, respectively), the microcrack density will decrease rapidly with distance from the crack tip. This is illustrated in Figure 4 for three values of m (2,6,12) and for a range of $K_I/S_o\sqrt{D_m}$ (where D_m is the average microcrack length, e.g. as determined by the average grain diameter), by plotting ρ/ρ_o as a function of r/D_m.

4.2 Effects on fracture toughness

4.2.1 Discrete microcrack model

A discrete two-dimensional microcrack model for the effect of microcracking on fracture toughness can be developed (using numerical methods), by assuming simplified crack geometries - such as grain boundary fracture in a hexagonal grain network (Figure 5a).

*A modification of the Batdorf and Crose analysis is required because they attempted to address the problem of first fracture in a volume V, whereas in the present problem we require a determination of the total number of fractures (see section 4.2).

**The major disparity between this assumed stress field and the principal tensile stress field (see Figure 2) occurs at $\pi/4 > \theta < -\pi/4$. However, in this range of θ the stress is strongly biaxial, which would cause the fracture probability in this zone to be larger than in the remainder of the zone, at the equivalent stress level [26]. The use of this assumed stress field, with a uniaxial fracture probability, might thus afford a better description of the actual microfracture densities than expected from the application of alternate angular dependencies.

This approach, as pioneered by McClintock and colleagues [27,28], entails defining a microfracture probability function that determines the probability of forming the first microcrack. This function differs from equation (8) because it pertains to the weakest element and must contain a dependence on the volume of material sampled. Several functions have been used for this purpose [1,26,29,30]. The most satisfying of these utilize the product of the probabilities of zero microfracture $\Pi_i(1-\delta\phi)_i$, in individual small elements, δV[1,27,28], when a stress S is applied *normal* to the prospective fracture plane

$$1 - \Phi_1 = \Pi_i(1-\delta\phi)_i = \Pi_i\ [1-\delta V_i \int_o^S g(S)\ dS] \tag{13}$$

where g(S) is any function that describes the observed stress dependence of microfracture. For a homogeneous stress field (uniaxial or polyaxial), the probability of first microfracture in a volume, V, then becomes;

$$\Phi = 1 - \exp\left[-V\int_o^S g(S)\ dS\right]. \tag{14}$$

The most frequently used g(S) function has a form suggested by extreme value statistics [1,24,27,28];

$$g(S) = \left(\frac{S-S_u}{S_o}\right)^m \tag{15}$$

where S_u, S_o and m are constants; it should be noted [26], however, that other g(S) functions may have a more fundamental significance. To determine the probability Φ of first microfracture in the stress field of a primary crack, the tensile stress in each element of the field, in a direction normal to the microfracture plane, is firstly deduced from the stress field functions (such as equation (3)) and combined with equation (13) to determine the probability of zero microfracture, $1-\delta\phi$, in that element. Then the product of, $1-\delta\phi$, over the entire stress field, $\Pi_i(1-\delta\phi)_i$, is evaluated. If the first microcrack has a high probability of being contiguous with the primary crack (at AB or AC in Figure 5a), then a significant microcrack zone will not develop, and there is a simple relationship between the microcrack formation parameters and K_c. However, if there is a high probability that the first microcrack forms at a position remote from the primary crack (Figure 5b), the analysis of the microcrack zone may proceed. The next step is to re-evaluate the stress field in the presence of the first microcrack. For this purpose, McClintock [28] has used a boundary integral method with the cracks being modeled by dislocation arrays which cancel the applied stress across the 'crack' plane. At this juncture two probability calculations must be performed; (i) the probability of formation of a second microcrack remote from the first microcrack, using the same procedure utilized to determine the formation of the first microcrack; and (ii), the probability that the second microcrack will be contiguous with the first. The latter is determined by noting that the pertinent stress intensity factor that relates to the formation of a contiguous microcrack is [28]

$$K = \frac{3}{8}\sqrt{3\pi}\ \sigma\sqrt{a} \tag{16}$$

and by defining an extreme value function for K similar in form to equation (14). Then by considering that microcracking is determined by the normal stress at a distance y from the microcrack tip, the probability of contiguous microcracking can be obtained. Thereafter, the cracking

process (contiguous or remote) with the larger probability is assumed to be the preferred mode of microfracture. The stress field is then re-evaluated in accord with the most probable event, and the entire process is repeated until a high probability of microfracture contiguous with the primary crack is realized, whereupon K is equated to K_c. This process is illustrated schematically in Figure 5b.

Some results obtained for isotropic ceramics using this procedure are summarized in Table II. These results provide some very important insights into the role of microfracture on the fracture toughness. The normalized toughness, $K_c/\bar{S}\sqrt{y}$, is determined primarily by the coefficient of variation (which is dictated by the distribution parameter m and, to a lesser extent, by S_o), but the range is relatively small, ~2.5. More important influences on the fracture toughness (than the microfracture variability) are thus likely to derive from the toughness normalization parameters, i.e. the microfracture strength level, $\bar{S}$ (which is determined primarily by S_o) and the microfracture location, y (which relates to microstructural parameters, such as the grain diameter D_g). A similar result is obtained from the continuum microcrack model (section 4.2.2), and the consequences are discussed in more detail in relation to that model. One additional result that derives from the discrete model is that microfracture anisotropy can greatly influence the role of microfracture on the fracture toughness. Specifically, when the grain boundaries parallel to the crack exceed ~3.5 times the strength of the orthogonal boundaries, extensive microfracture can occur on boundaries orthogonal to the macrocrack plane, and significant anisotropy toughening can then commence.

4.2.2 Continuum microcrack model

An alternate approach to the evaluation of microfracture uses continuum microcrack densities, derived in the manner discussed in 4.1. This approach does not have the two dimensional limitation of the discrete model, but (as discussed below) has the disadvantage that the condition for primary crack extension can only be defined in approximate form.

The microcrack distributions around a primary crack (Figure 4) can provide the rationale for a continuum microfracture analysis, by surmising that the microcracks in an inner zone ($r \leq D_m$) tend to interact (or link) with the primary crack [31], and thus provide the principal driving force for primary crack extension; whereas the microcracks in the outer zone, ($r > D_m$) which change the compliance (or effective modulus [22]) of the material in that zone (and, therefore, tend to reduce the crack opening displacement [32]), are the principal source of toughness enhancement.

For single phase ceramics, the microcrack density in the inner zone can continue to increase as K increases (see Figure 4). However, when a certain fraction (~0.5) of the grains have microcracked, the microcrack separation is small enough that interaction effects (i.e. the self interaction of the microcracks and their interaction with the primary crack) become important [31].

The microcrack density in this zone is then likely to increase at a substantially more rapid rate than indicated by the non-interacting result (Figure 4). Thereafter, primary crack extension should quickly ensue. Hence, setting the microfracture probability for $r < D_m$ equal to 0.5, provides an approximate crack extension condition. Thus, by specifying the microcrack density (equation 12) in an element rdr, integrating over

the inner zone

$$\Phi \equiv \frac{\rho}{\rho_o} = \frac{1}{D_m}\int_o^{D_m} r\left[1 - \exp\left(\frac{K_I}{2\pi\, S_o}\right)^m r^{-m/2}\right] dr \,, \qquad (17)$$

and setting the integral equal to 0.5, we obtain;

$$\frac{K_c}{S_o\sqrt{D_m}} = \xi(m) \,, \qquad (18)$$

where ξ is ≈ 2 for all reasonable values of m. This result could, in fact, have been anticipated from Figure 4, because $K/S_o\sqrt{D_m}$ is ≈ 2, at $r = D_m$, when $\Phi = 0.5$, for all three m values. This is not, however, the final result for the effect of microfracture on K_c, because the change in the stress field caused by the more compliant outer zone has not yet been included. A detailed analysis of the effect of this compliance change on the crack opening displacement has not yet been obtained, and the only available analyses that provide some insights are the solutions for a crack penetrating, and included in, an elastic inclusion [32,33]. These results indicate that the crack opening decreases (for a given stress and crack length) as the inclusion modulus decreases. Qualitatively, therefore, we presume that the crack opening decreases as the density of microcracks in the outer zone and the zone size increase, thereby causing a corresponding increase in toughness. It is then apparent from Figure 4 that the toughness enhancement can be optimized by decreasing m; although the extent to which K_c can exceed the value suggested by equation (18) is, as yet, indeterminate.

For two phase (or multiphase) ceramics, where microcracking occurs by the fracture of either the second phase particles or of the surrounding matrix (as determined by the relative expansion coefficients and moduli of the matrix and second phase [1]), the detrimental influence of inner zone microfracture can be avoided if the volume fraction of the second phase is maintained below the level where microcrack interaction effects become important [31] (i.e. ~0.5). Then, the advantages of the compliant microcrack zone can be fully realized, especially by selecting a second phase that maximizes the zone size (i.e. by establishing a wide dispersion, m, and a low microfracture strength, S_o, as indicated by Figure 4).

4.3 Microstructure dependence

4.3.1 Single phase ceramics

It is instructive for microstructural design purposes to examine the effects of the median grain size and the grain size distribution on the fracture toughness of materials that are susceptible to microcracking. Such materials are generally on non-cubic symmetry and exhibit appreciable elastic and thermal expansion anisotropy (e.g. alumina, silicon nitride). The fracture toughness derives directly from equation (18), as modified by the compliance of the outer microcrack zone. The grain size dependence of the microfracture stress (which can be approximately equated to S_o) is thus a key variable.

One approach for estimating the microfracture stress (based on a suggestion by Rice [23]) is to extend the energy balance arguments for particle microfracture used by Davidge and Green [34]. These arguments are based on the observation that particle microfracture is only *detected* when the strain energy attains a level consistent with the strain energy release being able to supply sufficient 'surface' energy for *complete* microfracture of the particle. The rationale for this observation might be similar to that used for Hertzian fracture, wherein it has been postulated [35] that a metastable precursor forms from the pre-existing defect (in accord with the usual critical strain energy release rate requirement), and that the precursor only grows to an observable size at a condition essentially coicident with the balance of strain and 'surface' energy being satisfied.

The 'surface' energy U_S generated by grain microfracture is

$$U_S \approx \frac{\pi}{2} D_g \Gamma_S \tag{19}$$

where Γ_S is the single crystal fracture energy. The strain energy release consists of two parts: the first derives from the thermal expansion mismatch U_α and an *upper limit* is given by [34],

$$U_\alpha \approx \frac{-\pi D_g^3 (\Delta\alpha\Delta T)^2 E}{6(1-\nu)} \tag{20}$$

where $\Delta\alpha$ is the difference in expansion coefficients and ΔT is the temperature range over which the thermal expansion mismatch develops; the second strain energy release, U_σ, derives from the applied stress, and for fixed grip conditions the upper limit is;

$$U_\sigma \approx \frac{-\pi\sigma_A^2 D_g^3}{12\ E} \tag{21}$$

A *lower* limit for the microfracture stress can be obtained by setting equation (19) equal to the sum of equations (20) and (21), giving

$$\sigma_A \gtrsim \sqrt{6\left[\left(\frac{E\Gamma_S}{D_g}\right) - \frac{(E\Delta\alpha\Delta T)^2}{3(1-\nu)}\right]} \tag{22}$$

Further, by defining D* as the grain diameter for spontaneous microfracture ($\sigma_A = o$), equation (22) can be simplified to

$$\sigma_A \gtrsim \sqrt{\frac{6\ E\Gamma_S}{D^*}\left(\frac{D^*}{D_g} - 1\right)} \tag{23}$$

Equating σ_A to S_o and letting $\sqrt{2E\ \Gamma_S} = K_S$ the single crystal fracture toughness, we obtain

$$\frac{K_c}{K_S} \gtrsim 2\sqrt{3\left(1 - \frac{D_g}{D^*}\right)} \tag{24}$$

Thus, neglecting compliance effects, the fracture toughness of the polycrystal relative to the single crystal decreases as the grain size increases,

as shown in Figure 6. This behavior could certainly be modified when the r duced modulus of the outer microcrack zone is incorporated in the crack extension analysis, especially for a wide grain size distribution (i.e. small m), where the compliance effect could be substantial. However, grain size distributions usually scale with the median grain size [36] (in the absence of secondary grain growth), and in most instances, the essential grain size effect predicted by equation (24) is likely to be retained. Typical grain size dependencies for elastically anisotropic materials [23] indicate that K_c does diminish at large grain sizes in accord with the prediction. However, there is also a decrease at small grain sizes, which could, in the context of the present model, be related to a corresponding decrease in K_S, being replaced by K_B for boundary fracture. Such an effect is consistent with the observation of a larger proportion of intergranular fracture at small grain sizes [37]; but it is also possible, of course, that the disparity signifies a deficiency in the present simplified model.

4.3.2 Multiphase ceramics

The potential advantages of microcracking for the generation of high toughness ceramics can be more effectively realized in multiphase than in single phase ceramics, because the microcrack density in the inner zone can be controlled by a judicious choice of the second phase material and its dispersion. For example, if the second phase is selected such that the particle itslef fractures, then it should be possible to include volume fractions up to at least 0.5 before inner zone interactions begin to degrade the toughness. Further, by choosing the size of the particles such that microfracture occurs at an optimum stress level,* a substantial microcrack zone and a large toughness can result.

Some of the most interesting work along these lines has been conducted recently by Claussen et al. [5]. Their work has entailed the design of alumina/zirconia systems which exhibit controlled microcracking. In this way, initial studies have produced materials with toughnesses, G_c, up to 240 Jm^{-2} and correspondingly good strengths. Also Hoagland et al [22] obtained very large toughness values on certain rocks (up to 1580 Jm^{-2}), which they attributed to microcracking. However, the fracture strengths of these latter materials were rather low, perhaps illustrating the primary deficiency of microcracking as a source of toughness in ceramics; viz., it may not be possible to generate a large toughness while maintaining a high fracture strength, because the requirements for high toughness (noted above) tend to oppose those for a large strength [28].

5. CRACK/PARTICLE INTERACTIONS

The presence of particles on or near the crack plane can impede the motion of the crack (Figure 7), thus causing crack "bowing" and a resultant increase in toughness. This crack bowing phenemenon was first postulated by Lange [38] and has recently been verified by Green et al [39] using an ultrasonic modulation technique.

*Although the size of the microcrack zone continues to increase as S_o decreases, the large toughness will not be reflected in a large fracture strength because the microcracks generate a critical macrocrack at relatively low applied stress levels [28]. The optimum S_o should thus be intermediate in value.

5.1 Toughening requirements

A second phase particle can only cause toughening if the particle is more resistant to crack propagation than the matrix. For a system in which the particle and matrix have comparable elastic, plastic and thermal expansion properties, a toughening can only be obtained if G_c for the particle exceeds G_c for the matrix. However, this situation is rarely achieved in practice, and more typical situations are discussed below.

a) *Brittle particles*

Generally, if the particles are brittle and have different physical properties than the matrix, localized stresses develop due to thermal expansion or elastic mismatch. The effect of these stresses on crack propagation can be estimated for conditions of small elastic mismatch using the same procedure adopted by Barenblatt to examine the non-linear cohesive zone [8,9]. Consider that the crack has to propagate through alternate zones of uniform tension, σ_T, and compression, σ_c, (corresponding to the particle and matrix, respectively), as shown in Figure 8a. To determine K for propagation through a compressive zone of length D_z, consider that this compression applies closure tractions over a length at the crack tip equivalent to the zone length (Figure 8b). Then, by the principle of superposition [8,9], we obtain;

$$K = K_o - \sqrt{\frac{2}{\pi}} \int_{a'-D_z}^{a'} \frac{\sigma_c dx}{\sqrt{a'-x}} \tag{25a}$$

$$\equiv K_o - 2\sigma_c \sqrt{\frac{2D_z}{\pi}} \tag{25b}$$

where K_o is the stress intensity factor due to the applied stress ($= \sigma_A \sqrt{\pi a'}$). Introducing the crack extension condition

$$K = K_{M,P} \tag{26}$$

where $K_{M,P}$ is the critical stress intensity factor for the matrix or the particle (depending on the location of the compressive zone), the applied stress intensity factor for crack propagation, K_c, becomes;

$$K_c = K_{M,P} + 2\sigma_c \sqrt{\frac{2D_z}{\pi}} \tag{27}$$

The equivalent result in the tensile zone is

$$K_c = K_{M,P} - 2\sigma_T \sqrt{\frac{2D_z}{\pi}} \tag{28}$$

For this simplified two-dimensional case, therefore, K_c will oscillate, as shown in Figure 8c, and the crack propagation resistance of the composite would be determined by the maximum K_c - at the compressive zone. This result suggests that a crack can be effectively impeded by the generation of large zones of compressive strain orthogonal to the crack trajectory. This effect is additive to any effects caused by differences in the toughness of the particle and matrix.

b) *Ductile particles*

When the second phase particles are ductile, significant localized stresses do not generally develop because they can be accommodated by deformation of the particles. However, a crack in the brittle matrix can circumvent the ductile particles leaving 'ligaments' across the crack faces, as shown in Figure 9, and these supply closure tractions which enhance the toughness of the material. The effects of these ligaments can be treated using the approach discussed above (as applied to a similar ligament problem by Dugdale [40]); but, in this case, the analysis is not confined to two dimensions. If we consider, for simplicity, a non-work hardening 'particle' material with a flow stress, σ_Y, and ductility (maximum strain to failure), ε_c, the force, F, exerted by each intact ligament of a cylindrical 'particle'* is

$$F \approx \frac{\pi \sigma_Y D_\ell^2}{4} \tag{29}$$

where D_ℓ is the diameter of the 'particle'. Then, by noting that the number of 'particles' per unit area, η, for a 'particle' deparation, d, is

$$\eta \approx \frac{1}{(D_\ell + d)^2} \tag{30}$$

the average compressive stress σ_c imposed by the ligaments becomes

$$\sigma_c \approx \frac{\pi \sigma_Y}{4\ (1+d/D_\ell)^2} \tag{31}$$

Substituting L, the length of the ligament zone (Figure 9), for D in equation (25b) and using equation (31) gives;

$$K = K_o - \sqrt{\frac{\pi L}{2}} \left(\frac{\sigma_Y}{(1+d/D_\ell)^2} \right) \tag{32}$$

The ligament zone length depends on the ductility and the effective gage length, ℓ, of the 'particles', as they affect the critical fracture displacement u_c. Hence, if the crack opening, u, is assumed to exhibit the following dependence on the distance, r, from the crack tip,

$$u \approx \frac{K_o}{2\bar{E}} \left(\frac{r}{2\pi} \right)^{1/2} R\left(\frac{r}{L} \right) \tag{33}$$

where R is a function of r/L (≈ 1 at r=L) and $\bar{E}$ is an effective modulus that depends on the modulus of both the matrix and ligament, equation (32) becomes;

*Spherical second phase particles are unlikely to be effective barriers to crack extension because the crack can merely propagate over them, through the matrix. A more effective dispersion would be a continuous network of ductile phase, perhaps along grain boundary triple points, as achieved for example in WC/Co alloys. Then each ductile 'particle' can be treated as a cylinder.

$$K \approx K_o - \pi \left(\frac{2u_c(\ell,\varepsilon_c)\bar{E}}{K_o} \right) \frac{\sigma_Y}{(1+d/D_\ell)^2} \qquad (34)$$

The critical applied stress intensity factor for crack propagation K_c (equal to K_o at fracture) is thus;

$$2K_c = K_m + \sqrt{K_m + 8\pi u_c(\ell,\varepsilon_c)\bar{E}\sigma_Y/(1+d/D_\ell)} \qquad (35)$$

where K_m is the fracture toughness of the matrix, as modified by the crack front bowing (see section 5.2). The important particle parameters affecting the toughness, all of which should be maximized, are thus the yield stress, the ductility, and the particle size. It is apparent from equation (35) that a substantial increase in toughness should be possible for quite moderate values of u_c and σ_Y. However, this approach to toughening is probably limited to materials that have application at relatively low temperature, because degradation of the metal at elevated temperatures would cause a corresponding diminution of the properties of the composite.

5.2 Magnitude of toughening

The exploitation of the toughening requirements suggested in the preceding section to produce ceramics with the maximum toughness requires that the three-dimensional aspects of the crack/particle interaction be introduced. This is particularly important for brittle dispersions (see section 5.1). The three-dimensional problem has not been solved, but approximate analyses [41,42] have provided some of the insights needed to understand the three-dimensional effects.

When crack/particle interactions occur, the crack bowing (Figure 7) causes K to be decreased at the leading portions of the crack front and to be enhanced at the trailing portions [41]. The magnitude of this effect for a single semicircular secondary crack is shown in Figure 10. It is apparent, therefore, that the maximum K_c values anticipated by two-dimensional analyses (e.g. Figure 8c) cannot be realized. The dispersion of the second phase and the profile that it presents to the crack is thus crucial to its potential as a source of toughness in all-brittle systems. One attempt to determine the role of the size and dispersion of the second phase, by calculating an approximate strain energy release rate for complete circumvention of an impeding zone [42] (i.e. the maximum possible toughening effect), gave the result plotted in Figure 11. This shows that the impeding zones must occupy a good fraction of the crack front if a significant toughening is to be realized.

Further progress in defining the potential of brittle dispersions for toughness enhancement is probably most effectively pursued by resort to data from actual systems. One notable example is a recent study [3] of the effects of coherent precipitation on the fracture toughness of zirconia/magnesia alloys. In the as-quenched (cubic solid solution) condition, the material has a toughness of ~ 2.8 MPa $\sqrt{m}$. By aging to achieve the formation of optimally sized coherent tetragonal zirconia particles, the toughness was increased to 5.9 MPa $\sqrt{m}$. Using the model of equation (27), it can easily be shown that a compressive strain of 2.5% is necessary to enhance the toughness of the matrix by this amount, assuming a zone size of 0.2 μm (Figure 12). (E for ZrO_2 alloys is ~ 172 GN/m^2). The ellipsoidal

particles shown in Figure 12, which precipitated with tetragonal symmetry on aging at 1400 °C [3], inverted to the monoclinic form in the stress field of the crack. This phase transformation involves a $\sim 3\%$ anisotropic volume expansion, which causes a complex pattern of strains in both the matrix and the particles. Analysis of these strains [3] using a method suggested by Eshelby [43] indicated *local* compressive strains as large as 15%, and strains of 1-6% appeared to exist over large areas of the matrix, along the principal axes of the particles. The strain of 2.5% suggested by equation (27) thus appears to be a sensible average. Thus the three-dimensional nature of the precipitation (Figure 12) did in fact generate compressive zones that effectively impeded the crack over a large portion of its length.* Further studies of this, and related phenomena are in progress.

This approach to toughening thus looks very promising, and does not have the disadvantage associated with microcracking, that the microstructural changes that enhance the toughness also limit the fracture strength. In fact, it is entirely possible for the strength to be increased in direct porportion to the increase in fracture toughness.

6. OTHER MECHANISMS

6.1 Phase transformations

It has been suggested that toughening in certain ceramics [4] can be achieved if a phase transformation can be induced by the stress field of the crack. This can only be effective (see above), if the transformation reduces the tensile stress orthogonal to the plane of the primary crack. The phase transformation is thus simply a method for introducing the localised compression discussed in 5.1.a. A simplified example of how this might occur, for a shear transformation, is illustrated in Figure 13.

6.2 Pull-out

The relatively high toughness of hot pressed silicon nitride has been attributed to the 'pull-out' of elongated grains [44], as illustrated in Figure 14. Such a mechanism could apply if the fracture resistance of the elongated grains on planes normal to their major axis is large and the shear strength of the interface, τ_i, is relatively small. (Then pull-out rather than transgranular fracture is encouraged). The mechanism might thus apply to hexagonal materials fabricated by a liquid phase sintering technique, which would promote the growth of grains elongated along the c-axis, thereby exposing the most fracture resistant (basal) plane to the crack [45], and would leave a grain boundary 'residue' which could reduce the shear resistance of the boundary.

The mechanics of this process can be treated in a manner analogous to the ligament problem used to evaluate the effect of ductile particles (section

*One alternate explanation for the toughness is that microcracking is also occurring. We consider this to be unlikely because the microfracture stress level, S_o, for this system is very large.

5.1b). Here, however, the closure tractions are determined by the shear strength of the interface. For cylindrical grains of length, ℓ, and diameter, D_ℓ, the compressive force, F, per grain is

$$F = \frac{\pi D_\ell}{2}\left(\frac{\ell-u}{2}\right)\tau_i \qquad (36)$$

Combining this with the average number of grains per unit area (equation 30) gives the average compressive stress

$$\sigma_c = \frac{\pi}{2}\frac{(\ell-u)\,\tau_i}{(1+d/D_\ell)^2 D_\ell} \qquad (37)$$

where d is the average separation of elongated grains. Then the critical stress intensity factor can be obtained from equaiton (25b) as;

$$K_c \approx K_m + \tau_i\sqrt{\pi L(\ell)}\,\frac{[\ell-\tilde{u}]}{(1+d/D_\ell)^2 D_\ell} \qquad (38)$$

where L is the length of the pull-out zone (which is a function of the grain length, ℓ) and $\tilde{u}$ is the separation of the crack faces* in the ligament zone. The toughness thus increases as the interface shear strength increases. However, there is a limitation to the toughening that can be effected by increasing the interface shear strength, imposed by the onset of grain fracture, which occurs at a stress, σ_f. Grain fracture intervenes when

$$(\tau_i \ell)_{max} \gtrsim 2\sigma_f \qquad (39)$$

and since there is a high probability of grain fracture at a site relatively close to the crack surface, the pull-out length will thereafter, be much less than ℓ. Grain fracture thus coincides with a sharp decrease in the value of the second term in equation (38). However, this decrease could be partially or wholly counteracted by the increase in the first term, which now includes a grain fracture contribution. Since the relative importance of these counteracting terms cannot yet be ascertained, it is premature to conclude that toughening can, in fact, be achieved by encouraging grain pull-out. However, should such a toughening mechanism be confirmed it is then apparent from equations (38) and (39) that the fracture strength of the elongated grains should be as large as possible; while the interface shear strength should have an intermediate value dictated by the grain length.

7. CONCLUSION

The primary toughening mechanisms that apply to polycrystalline ceramic materials have been examined. The mechanisms which appear to have the greatest general scope for *major* increases in toughness are (i) the inclusion

*A detailed analysis would require that u(x), c.f. equation (33), be used for $\sigma_c(x)$, which would then be integrated (in equation 25a) to obtain K. However, since u(x) is not easily determined, a simplified form of the analysis is presented herein, which can be used to identify the primary toughening requirements.

of brittle second phase particles that microcrack in the stress field of the primary crack, and (ii) the use of a continuous network of a ductile phase. Both of these approaches have limitations, however. The microcrack approach to enhancing toughness does not lead to an equivalent increase in the fracture strength because the microfracture parameters that govern these two properties are opposite in character. The use of a ductile second phase, on the other hand, limits the material to relatively low temperatures, and thus does not take full advantage of the desirable properties of the ceramic.

The other approach that appears very promising is the use of coherent precipitates etc. to induce extensive zones of compression orthogonal to the crack plane. This approach should lead to equivalent increases in strength and toughness and should also be adaptable to materials with good high temperature stability (as effected by a judicious choice of the alloy system). The maximum toughening that can be realized is, however, more limited in scope than the microcracking or ductile second phase approaches.

Finally it should be emphasized that the toughening approaches discussed herein should not necessarily be considered separately; the concurrent use of several toughening mechanisms may yield the optimum properties.

ACKNOWLEDGEMENTS

The authors wish to thank Dr. A. W. Thompson for reading an earlier version of this manuscript. We also thank Drs. McClintock, Rice and Claussen for making available their research results and analyses prior to publication. Finally, one of us (AGE) acknowledges the financial support of the Rockwell International Independent Research and Development Program and the others acknowledge the support of N.S.F.

REFERENCES

1. EVANS, A.G. and LANGDON, T.G., Progress in Materials Science, 19, 1976.
2. McCLEAN, A. F., FISHER, E. and BRATTON, R. J., Brittle Materials Design, High Temperature Gas Turbine, ARPA Reports AMMRC CTR, 1971-76.
3. PORTER, D. L. and HEUER, A. H., work performed at Case Western Reserve University, to be published.
4. GARVIE, R. C., HANNINCK, R. H. and PASCOE, R. T., Nature, 258, 1975, 703.
5. CLAUSSEN, N. and STEEB, J., work performed at Max-Planck-Institut, to be published.
6. FREIMAN, S. W., RICE, R. W. and McDONOUGH, W. J., Bull. Am. Ceram. Soc., 55, 1976, 396 (abstract only) to be published.
7. RICE, J. R. and THOMSON, R., Phil. Mag., 29, 1974, 73.
8. LAWN, B. R. and WILSHAW, T. R., Fracture of Brittle Solids, Cambridge University Press, Cambridge, 1975.
9. BARENBLATT, G. I., Adv. Appl. Mech. 7, 1962, 55.
10. EVANS, A. G., Scripta Met., 10, 1975, 93.
11. BURNS, S. J., Trans. Met. Soc. AIME, 236, 1966, 1165.
12. CLARKE, F.J.P., SAMBELL, R.A.J., and TATTERSALL, H. E., Phil. Mag., 7, 1962, 393.

13. WIEDERHORN, S. M., MOSES, R. L. and BEAN, B. L., Jnl. Amer. Ceram. Soc., 53, 1970, 180.
14. FREIMAN, S. W., BECHER, P. F., and KLEIN, P. H., Phil. Mag., 31, 1975,
15. ALQUIST, C. N., Acta Met. 22, 1974, 1133.
16. STROH, A. N., Adv. Phys. 6, 1957, 418.
17. WIEDERHORN, S. M., HOCKEY, F. J., and ROBERTS, D. W., Phil. Mag., 28, 1973, 783.
18. EVANS, A. G. and WIEDERHORN, S. M., Jnl. Mater. Sci., 9, 1974, 270.
19. EVANS, A. G. and LANGE, F.R., Jnl. Mater. Sci., 10, 1974, 1659.
20. EVANS, A. G., LINZER, M., and RUSSELL, L. E., Mater. Sci. Eng., 15, 1972, 253.
21. EVANS, A. G. and LINZER, M., Jnl. Amer. Ceram. Soc., 56, 1972, 575.
22. HOAGLAND, R. G., HAHN, G. T., and ROSENFIELD, A. R., Rock Mechanics, 5, 1973, 77.
23. RICE, R. W. and FREIMAN, S. W., Bull. Amer. Ceram. Soc., 55, 1976 394 (abstract only) to be published.
24. GUMBEL, E., Statistics of Extremes (Columbia University Press) N.Y., 1956.
25. EVANS, A. G., CLIFTON, J. R., and ANDERSON, E., Cement and Concrete Research, 6, 1976, 535.
26. BATDORF, S. and CROSE, J. G., Jnl. Appl. Mech. 41, 1974.
27. McCLINTOCK, F. A. and MAYSON, H.J., ASME Applied Mechanics Conf., June 1976, to be published.
28. McCLINTOCK, F. A. and ZAVERL, F., Intl. Jnl. Frac., to be published.
29. McCLINTOCK, F. A., Fracture Mechanics of Ceramics (ed. R. C. Bradt, F.F. Lange and D.P.H. Hasselman) Plenum, N.Y., 1974, 93.
30. WEIBULL, W., Jnl. Appl. Mech., 18, 1951, 293.
31. EVANS, A. G. and CHARLES, E. A., Acta Met., to be published.
32. ERDOGAN, F., Fracture Mechanics of Ceramics, ibid, p. 245.
33. ERDOGAN, F. and GUPTA, G., Intl. Jnl. Frac., 11, 1975, 13.
34. DAVIDGE, R. W. and GREEN, T. J., Jnl. Mater. Sci., 3, 1968, 629.
35. FRANK, F. C. and LAWN, B. R., Proc. Roy. Soc., 299, 1957, 291.
36. MARCHANT, D. D. and GORDON, R. S., Jnl. Amer. Ceram. Soc., 55 1972, 19.
37. GUTSHALL, P. L. and GROSS, G. R., Eng. Frac. Mech., 1, 1969, 463.
38. LANGE, F. R., Phil. Mag., 22, 1970, 983.
39. GREEN, D. J., NICHOLSON, P. S. and EMBURY, D., Bull. Amer. Ceram. Soc., 55, 1976, (abstract only) to be published.
40. DUGDALE, D. S., Jnl. Mech. Phys. Solids, 8, 1960, 100.
41. EVANS, A. G. and GRAHAM, L. J., Acta Met., 23, 1975, 1303.
42. EVANS, A. G., Phil. Mag., 26, 1972, 1327.
43. ESHELBY, J. D., Proc. Roy. Soc. A241, 1957, 376.
44. LANGE, F. F., Jnl. Amer. Ceram. Soc., 57, 1974, 84.
45. WIEDERHORN, S. M., Jnl. Amer. Ceram. Soc., 9, 1969, 485.

TABLE I - Summary of toughening mechanisms for ceramics.

TOUGHENING MECHANISMS	COMMENTS
1. Increase Dislocation Flow Stress	Applies to Materials in Which Crack Extension is Dislocation Assisted
2. Microcrack Formation or Extension Activated by Stress Field of Crack	Can Increase or Decrease Toughness
3. Crack/Particle Interaction	Applies if Particle can Impede Crack Extension
4. Phase (or Coherent → Incoherent) Transformation of Second Phase Induced by Stress Field of Crack	
5. Pull-out of Elongated Grains	

TABLE II - Effects of microfracture on fracture toughness of an isotropic polycrystal, [two-dimensional discrete model (McClintock and Zaverl)].

COEFFICIENT OF VARIATION ($\sigma/\bar{S}$)	NORMALIZED TOUGHNESS, ($K_c/\bar{S}\sqrt{y}$)
0	1
0.06	2.1
0.12	2.6
0.18	2.4
0.28	2.1
0.38	2.0

$\bar{S}$ is the *average* microfracture strength

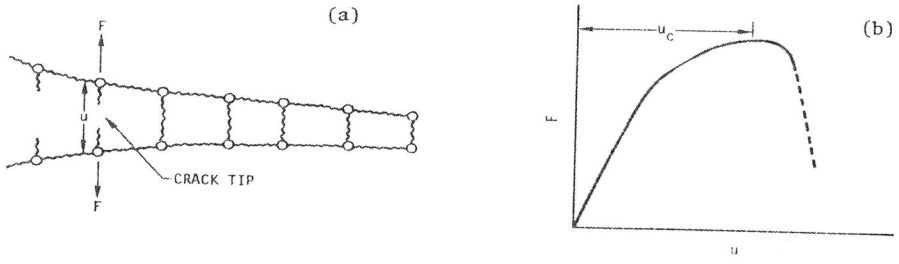

Figure 1 (a) Sketch of the bond rupture process at a crack tip.
(b) A possible force, displacement curve for bond rupture. u_c is the critical displacement for bond rupture.

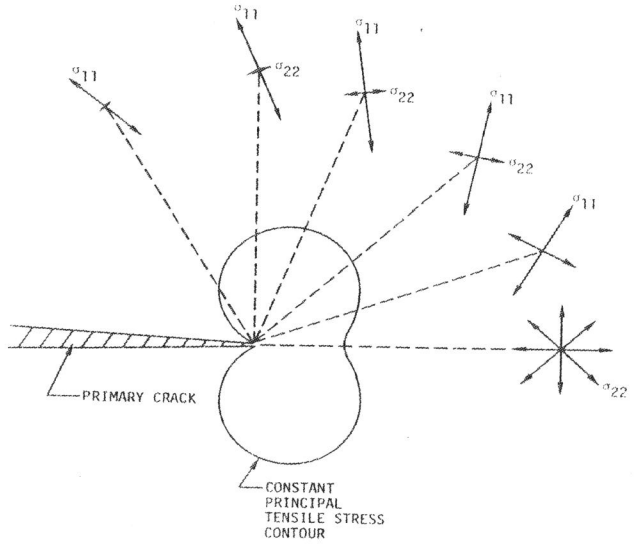

Figure 2 The principal tensile stress magnitudes and orientations at several angles taken around a crack tip; also shown is a constant principal tensile stress contour.

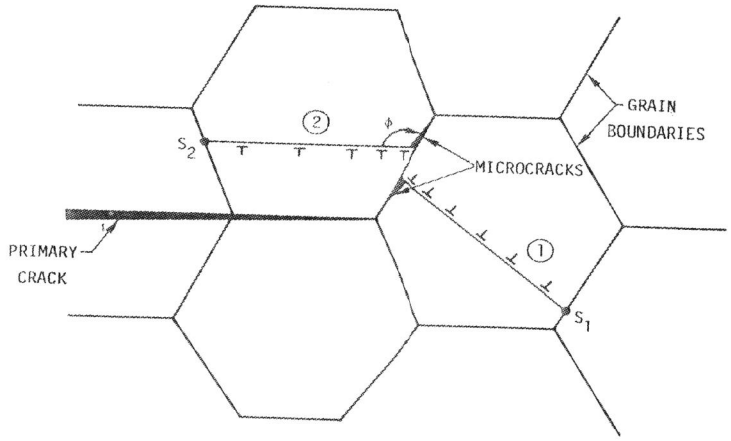

Figure 3 Two possible dislocation pile-up conditions that could generate microcracks and lead to dislocation-assisted crack propagation in ceramic polycrystals.

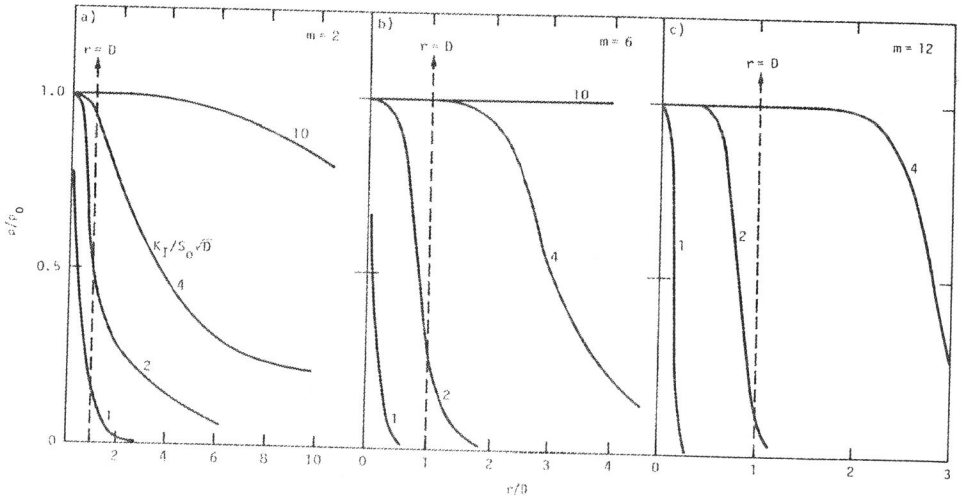

Figure 4 Relative microcrack densities as a function of normalized distance (r/D_m) from the crack tip as a function of the normalized stress intensity factor ($K/S_o\sqrt{D_m}$) for three values of the scale parameter, m.

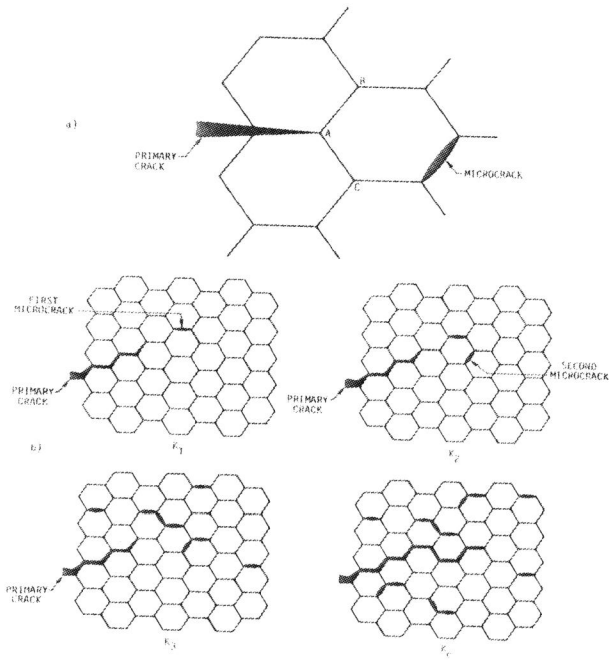

Figure 5 (a) A hexagonal grain network used for the discrete model of micro-fracture effects on toughness.

(b) A schematic of the sequence of events (as a function of K) that constitute macrocrack propagation in a material that is susceptible to microfracture.

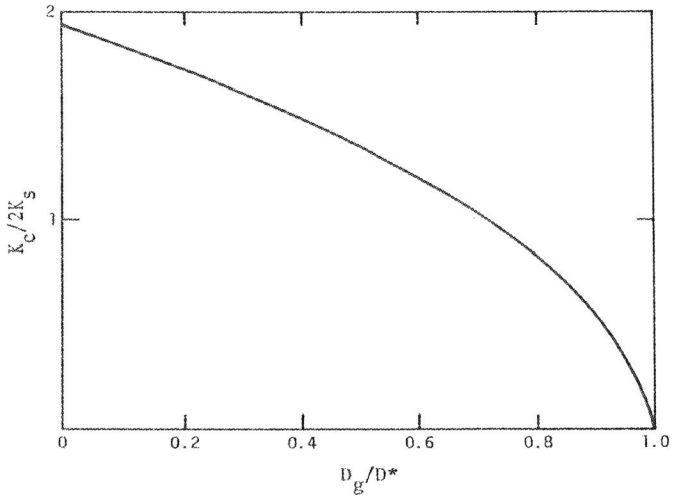

Figure 6 The effect of grain size on the fracture toughness of a ceramic polycrystal that is susceptible to micro-fracture induced by thermal expansion anisotropy.

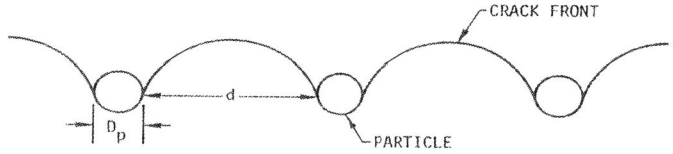

Figure 7 A schematic of a crack bowing between obstacles.

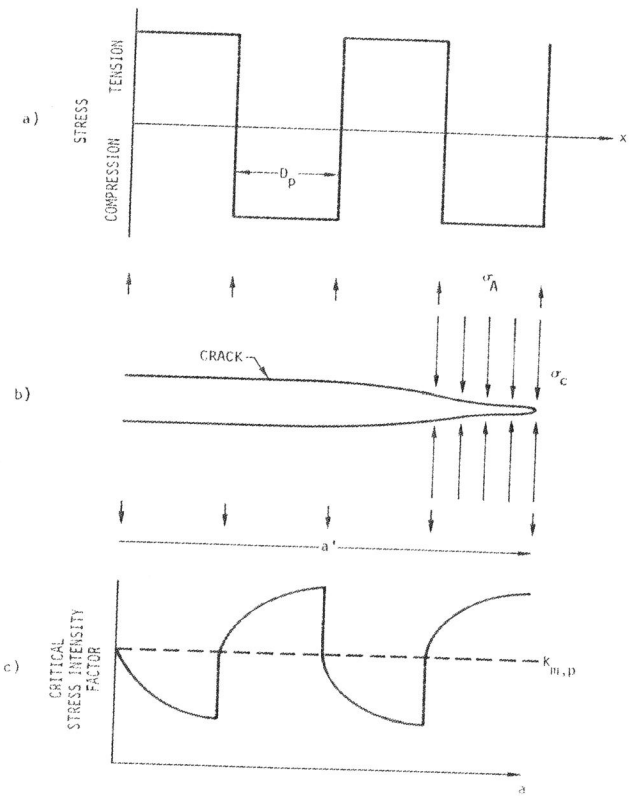

Figure 8 (a) A schematic of alternating tensile and compressive zones induced by lattice mismatch strains.

(b) The stress system imposed on a crack as it propagates through a compressive zone.

(c) The stress intensity factor variations that correspond to the stress variations shown in (a).

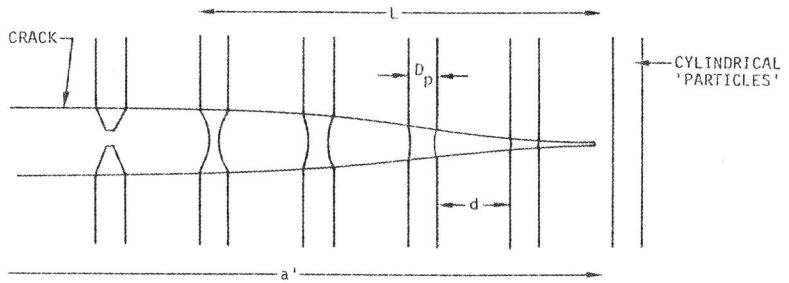

Figure 9 A schematic of a crack 'bridged' by ductile 'particles'.

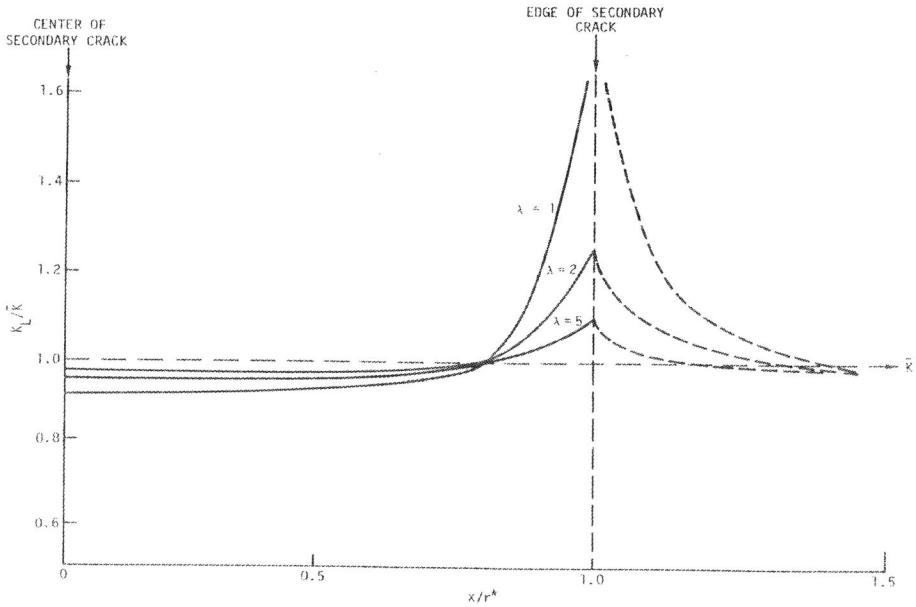

Figure 10 The approximate variation in K across secondary cracks with three aspect ratios, λ. [41]

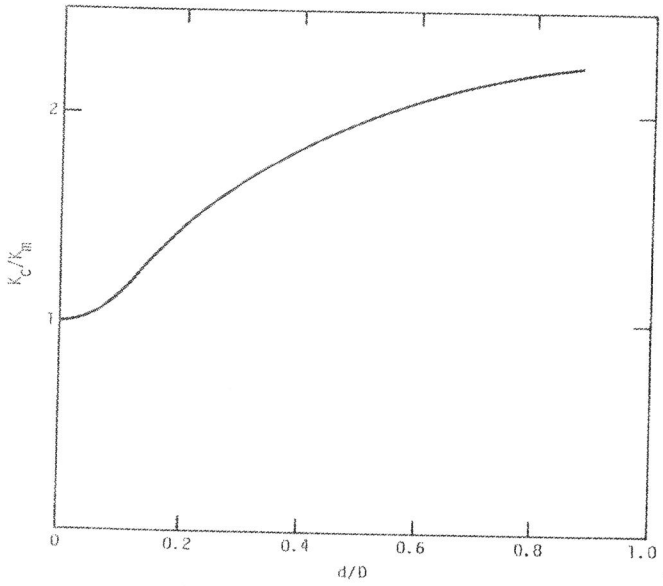

Figure 11 The maximum effect of the relative obstacle spacing on the toughness, for complete obstacle circumvention.

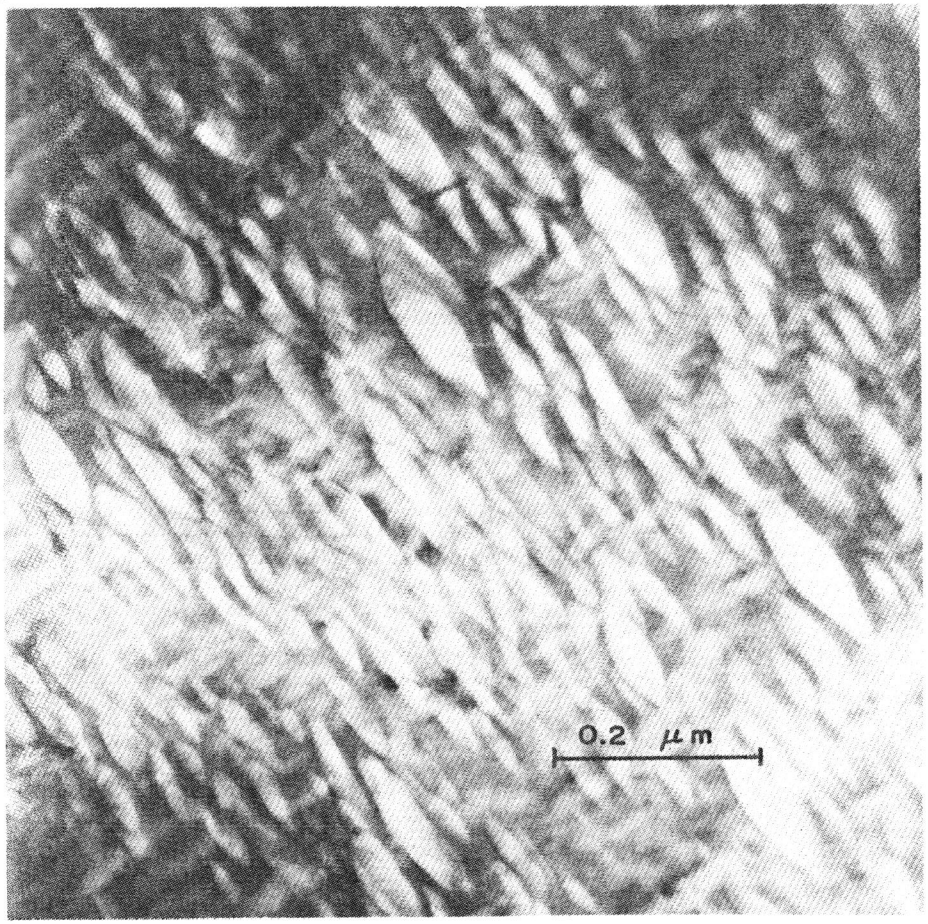

Figure 12 A transmission electron micrograph of coherent tetragonal zirconia particles in a cubic zirconia/magnesia matrix.

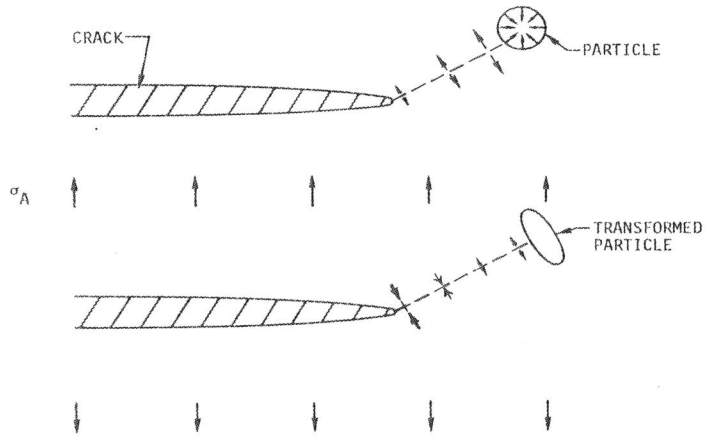

Figure 13 A schematic of a phase transformation, induced by the stress field of a primary crack, which could enhance the fracture toughness.

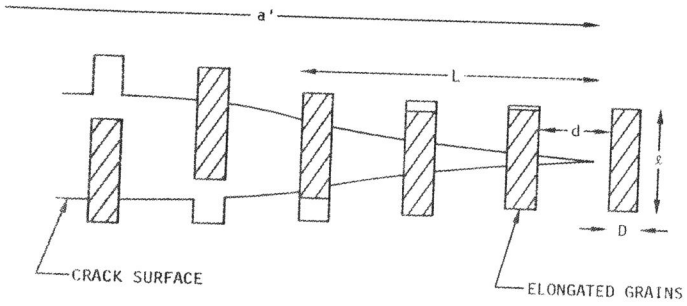

Figure 14 A schematic of the pull-out of elongated grains.